Final Draft
of the original manuscript:

Srinivasan, P.B.; Dietzel, W.; Zettler, R.; dos Santos, J.; Sivan, V.:
Effects of inhibitors on corrosion behaviour of dissimilar aluminium alloy friction stir weldment
In: Corrosion Engineering Science and Technology (2007) Maney

DOI: 10.1179/174327807X159916

Effect of inhibitors on the corrosion behaviour of a dissimilar aluminium alloy friction stir weldment

P Bala Srinivasan[a,*], W Dietzel[b], R Zettler[b], JF dos Santos[b] and V Sivan[a]

[a]Department of Metallurgical and Materials Engineering
National Institute of Technology
Tiruchirappalli 620 015, India

[b]GKSS-Forschungszentrum Geesthacht GmbH, Institute for Materials Research
D-21502 Geesthacht, Germany

Abstract

Dissimilar weldments comprising age hardenable AA7075 and AA6056 aluminium alloys were produced by friction stir welding. Corrosion behaviour of the weld nugget/TMAZ region and parent materials were characterised in chloride solutions. Chromate, molybdate and cerium nitrate additions were made to the chloride solution and their effect on the corrosion behaviour of weldment was assessed. The electrochemical studies on the different regions of the dissimilar friction stir weldment, performed in 3.5% solutions suggest that chromates are better in terms of inhibition efficiency, and a more or less similar beneficial effect on the corrosion resistance was received by all the regions by the addition of chromate inhibitor. From the view point of environmental issues, both molybdate and cerate can be thought of as inhibitor; however, their efficiency levels are definitely below that of chromates in neutral chloride environments.

Introduction

Aluminium alloys find extensive applications in aerospace, aircraft, defence and structural applications. The use of heat treatable aluminium alloys in all these sectors is ever-increasing owing to their excellent strength to weight ratio and

* Corresponding author
Phone: 00-91-98940 27520; Fax: 00-91-431-2500 133; email: pbs@nitt.edu

reasonably good corrosion and environmental cracking resistance. The joining of aluminium alloys has been carried out with a variety of fusion and solid state welding processes. However, the friction stir welding (FSW), a solid state joining process, developed by The Welding Institute (TWI), UK, has demonstrated very high suitability for the joining of aluminium alloys [Thomas et al., 1991]. Although this joining process is, relatively, a recent development, it has found its applications in many areas, and has particularly aroused the interest of the aircraft, aerospace and automotive industries owing to its capability of producing sound joints even in age hardenable aluminium alloys, which are considered problematic with regard to weldability [1,2]. The fact that the bonding in FSW occurs with the base materials remaining in the solid state offers a great potential to produce joints between the so-called difficult-to-weld heat treatable aluminium alloys. The weld joints produced by FSW have been reported to have joint efficiencies ranging from 80% – 100%, in terms of tensile properties [3 – 5]. A good number of publications are available in the literature concerning the microstructural evolution and the associated structure-property correlation of friction stir welds for similar alloys [6 – 9] and some information with regard to dissimilar alloy combinations has also been published in recent times [10 – 11]. However, there are only a few reports on the corrosion behaviour of friction stir weldments [12 – 14], and most of these have focused on joints similar alloy weld joints. This work addresses the corrosion behaviour of a dissimilar friction stir weldment comprising two grades of age-hardenable aluminium alloys viz., AA7075 and AA6056.

Experimental

Aluminium alloy plates of 5 mm thickness – AA7075-T7351 (5.7% Zn, 2.4% Mg, 1.6% Cu, 0.4% Si, balance Al) and AA6056-T4 (1.1% Si, 1.0% Mg, 0.90% Cu, balance Al) – were employed in this investigation. Welds were produced using

a robotic friction stir welder with the following welding parameters: tool rotation speed – 900 rpm; force – 11.5 kN; traverse speed – 250 mm·min^{-1}. The friction stir-welding tool comprised a tapered and profiled welding pin having a shank diameter of 5 mm and a concave shoulder profile of 15 mm diameter. Pin stick out was 4 mm as this was the length of the profiled region of the pin, meaning that the welds were produced shall have a lack of penetration between 0.60 mm to 0.90 mm.

Specimens for the macro and microstructural examinations were prepared by polishing successively with 220, 320, 400, 800, 1000 and 1200 grit emery papers, followed by disc polishing utilising 6 μm and 3 μm diamond slurry. Specimens were etched with Flick's reagent (15 ml HCl, 10 ml HF, 90 ml H_2O) for 45s to reveal the microstructural features.

The general corrosion behaviour of different regions of this dissimilar friction weldment was assessed in 3.5% NaCl solution. Based on the preliminary experiments, specific concentrations of chromates, cerium nitrate and sodium molybdate were chosen as inhibitors. Also, the specimens were given a chromate conversion coating in a conventional yellow chromating solution [15], and assessed for the corrosion behaviour in 3.5% NaCl solution and comparisons were made with inhibitors.

Further, the pitting behaviour of the different regions was assessed in 3.5% NaCl containing 0.01 M NaOH. All the electrochemical studies were performed in a computer controlled ACM Gill AC potentiostat using a three electrode cell. The sample, platinum electrode and a calomel electrode were made as working, auxiliary and reference electrodes, respectively. All the experiments

were performed at a scan rate of 0.5 $mV.s^{-1}$ and at ambient conditions (30±2°C).

Results and Discussion

Microstructure

The microstructural features of the AA6056-T4 and AA7075-T7351 base materials are shown in **Figures 1(a) and (b)**. Both these alloys exhibited un-recrystallised, elongated grain structure, but the AA7075 alloy had grains with a higher grain aspect ratio when compared to the AA6056 alloy. The globular dark dispersoids seen in the AA6056 alloy have been reported to be Al-Mg-Si containing intermetallic particles, richer in Si/Mg [16], whilst those in the AA7075 alloy were identified as Al_2Cu_2Fe, $Al_{23}CuFe_4$ (or) Al_2CuMg [13,17]. Though the intermetallic particles in these alloys could be observed by optical microscopy, the strengthening precipitates Mg_2Si and $MgZn_2$ in AA6056 and AA7075 alloys, respectively, could not be resolved by optical microscopy owing to their much finer size.

Optical macrograph of the weldment shown in **Figures 2** reveals the features of the geometry of the weld nugget and also of the adjoining regions of the weldment, showing the degree of mixing of the two materials and the flow patterns evolved in the weld nugget.

The microstructural features at the interface between the weld nugget and thermo mechanically affected (TMA) zones on either side of the weldment are presented in **Figures 3(a) and (b)**. The optical micrograph of the weld nugget, **Figures 4**, reveals that the flow and mixing of materials during the friction stir processing has resulted in a wavy-interlocking structure. As is expected in

FSW, the weld nugget region has shown a very fine and recrystallised grain structure. However, there existed differences in the grain size within the nugget, which is interesting. The region marked **'a'** in Figure 4 has shown a much finer re-crystallised grain structure compared to the light etched region marked **'b',** and the higher magnification micrographs shown in **Figures 5 (a) and (b)** clearly bring out the differences in the grain size in the respective regions. A closer examination showed that these regions 'a' and 'b' correspond to layers of AA7075 and AA6056 materials, respectively, evolved during the process of joining. Furthermore, the differences in the grain size within the nugget could be attributed to the initial grain sizes of the respective base materials.

The qualitative EDS line scan analysis performed in these zones revealed the differences in chemical composition within the weld nugget **(Figure 6)**, and further confirmed that the regions marked as (a) and (b) in Figure 4 correspond to the AA7075 and AA6056 alloys, respectively. The mechanical mixing of materials at elevated temperatures has led to the evolution of a fine grained recrystallised structure; however, the inherent differences in chemistry observed within the nugget region clearly suggests that the dwell time at these temperatures was insufficient for diffusion of alloying elements during friction stir processing.

Corrosion behaviour

The general corrosion resistance of the AA7075 and AA6056 parent materials and the weld nugget/TMAZ region were assessed in 3.5% NaCl solution (in the as-prepared condition) by potentiodynamic polarisation technique. No attempt was made to assess the corrosion behaviour of HAZ regions of this weldment, as the HAZ regions were very narrow and difficult to delineate macroscopically.

The effect of various inhibitors on the corrosion behaviour of different regions was also assessed in the same chloride environment. In addition, the pitting potentials were determined by performing polarisation studies in alkaline 3.5% NaCl test solution.

The potentiodynamic polarisation behaviour of the two parent materials and the weld nugget region assessed in 3.5% NaCl solution is presented in **Figure 7** and the electrochemical data are presented in **Table 1**. The open circuit potentials of the AA6056, AA7075 alloys and the weld nugget/TMAZ regions were observed to be –658.3 mV, –747.2 mV and –783.0 mV vs. SCE, respectively. The AA6056 alloy has exhibited a corrosion current density of 0.69 $\mu A.cm^{-2}$, as against values of 3.71 $\mu A.cm^{-2}$ and 3.32 $\mu A.cm^{-2}$ for the AA7075 alloy and nugget/TMAZ regions, respectively.

The mechanism of corrosion of aluminium and aluminium alloys in neutral and near-neutral aqueous solutions is based on the dissolution from active sites or flawed regions of the naturally formed barrier film. Both oxygen reduction to hydroxyl ions and hydrogen evolution are the prevalent cathodic reactions in these solutions, and metal dissolution is the anodic counterpart. The net reaction on the electrode surface results in the formation of $Al(OH)_3$, which in turn transforms to $Al_2O_3.3H_2O$, leading to passivity. However, in the presence of chloride ions, in addition to aluminium hydroxide formation, adsorption of chloride ions on the surface results in formation of soluble aluminium chloride ($AlCl_3$) which incidentally goes into solution, leading to hydrolyses and subsequent creation of active sites for further dissolution. The dissolution of the aluminium alloys is said to be dependent on the alloying elements,

secondary phases and/or precipitates in the alloy system, and also on the heat treatment condition.

The strengthening precipitate observed in AA6056 alloy is Mg_2Si and the electrode potential of this precipitate is not much different from the aluminium alloy matrix [18], hence the corrosion resistance observed is the highest among the three regions. On the other hand, the zinc rich precipitates in the AA7075 alloy causes the formation of micro galvanic cells, leading to higher rates of dissolution. Further, zinc is active when compared to aluminium alloy matrix, hence can enhance the corrosion rate. The higher corrosion rate of weld nugget regions is plausibly due to the fine grain size and the consequent increase in grain boundary area in the weld nugget region, and also the presence of some active precipitates in the matrix.

The steep increase in the current in the anodic side of the polarisation plot for all the three regions indicates that the pitting potentials are closer to their rest potentials in this test medium. Further, a much negative potential observed for the weld nugget/TMAZ region suggests that this regions could well be prone for attack under galvanic conditions, despite the fact that the general corrosion current density is lower than that of the AA7075 alloy.

The corrosion behaviour of the dissimilar weldment in 3.5% NaCl solution containing 0.2% Na_2CrO_4 and 0.3% $Na_2Cr_2O_7$ is depicted in **Figure 8** and the electrochemical data are given in **Table 2**. The addition of small amounts of chromates to the solution has shifted the corrosion potential of the different regions towards the active side. The improvements in corrosion resistance provided by the addition of chromates is seemingly significant, as could be

observed from the drastic reduction in corrosion current densities of the alloys compared to that in 3.5% NaCl solution without chromates. The effect of inhibition is observed to be more prominent in the 7075 alloy and in the nugget/TMAZ regions than in AA6056 alloy.

Interestingly, the anodic region of the polarisation plots for all the regions were observed to show a small region of pseudo-passivation, with a distinct breakdown at a higher potential than the rest potential. The role of chromate ions as a passivator for aluminium alloys can be explained by their powerful oxidising properties and good adsorbability [19] to the material's surface. The reduction of $Cr_2O_7^{-2}$ in to Cr (III) has been reported to be responsible for formation of Cr_2O_3 and Cr in the barrier film formed [20, 21]. Thus the presence of $Cr_2O_7^{-2}$ in the solution, even in solutions containing aggressive anions like chlorides, stimulates the repair of flawed regions of the surface film and oxidises the active site, resulting in the formation of stable corrosion resistant barrier film. From the electrochemical data presented in Table 5.2 it can be inferred that the corrosion resistance of all the three regions is significantly lower than their counterparts in 3.5% NaCl solution.

The polarisation behaviour of the weldment regions in chloride solution containing molybdate ions is presented **Figure 9** and the electrochemical parameters are provided in **Table 3**. The addition of molybdate has influenced the rest potential of AA6056 alloy and the weld nugget regions significantly. However, there was not much of change in the rest potential of AA7075 alloy compared to that in 3.5% NaCl solution without molybdate. The corrosion resistance offered by molybdate ions as inhibitors has been found to be relatively appreciable for the case of the weld nugget/TMAZ region and

AA6056; however, the effect is not very much pronounced in the case of AA7075 alloy. When compared to the inhibition effect provided by dichromates, the effect of molybdates is very much inferior. The remarkable difference between MoO_4^{2-} and $Cr_2O_7^{2-}$ as passivators is attributed to the weaker oxidising properties of MoO_4^{2-} when compared to that of $Cr_2O_7^{2-}$ and its tendency for polymerisation in neutral media [22], leading to bulky anionic species like $Mo_6O_{21}^{6-}$ which cannot accommodate easily in the flawed regions of the surface film during the anodic dissolution process.

The corrosion behaviour of the of the regions of weldment in chloride solution containing 0.01M cerium nitrate is shown in **Figure 10** and the associated electrochemical data are provided in **Table 4**. The open circuit potentials of all the three regions have been shifted towards the nobler side in this test medium in the presence of cerate ions. Unlike the earlier three cases, the corrosion potential of the weld nugget/TMAZ region has been observed to be shifted to values intermediate between that of the AA6056 and AA7075 alloys in this solution. The presence of cerium nitrate seems to have an appreciable effect on the corrosion resistance of the AA7075 alloy and the weld nugget/ TMAZ region. However, the overall inhibition efficiency of cerium nitrate has been found to very insignificant for the AA6056 alloy.

Cerium nitrate as inhibitor has been tried by researchers and the reports indicate that inhibition effect is comparable to that of chromates for zinc and zinc based alloys. Cerium chloride and nitrate have been attempted as inhibitors for aluminium alloys and only marginal improvements in general corrosion resistance have been reported. However, a better inhibition effect observed for the AA7075 alloy in the current case could possibly on account of

the presence of higher amounts of zinc. In all the three cases, despite the shift in the potentials towards the nobler side, the anodic (dissolution) behaviour of the samples are observed to activation controlled, and as of the case in 3.5% NaCl solution the pitting potentials were very much closer to their respective rest potentials.

The weldment was chromated in a yellow-chromating solution [15, 23] and the corrosion behaviour of the chromated specimens assessed in chloride solutions is presented in **Figure 11**. The effect chromate films in providing the corrosion resistance is well known and as can be noticed form the figure and the electrochemical data in **Table 5**, the chromate film has improved the corrosion resistance of all the three regions of this friction stir weldment, too. The effect is very significant in the AA6056 parent material, which has registered a corrosion current density of 0.048 $\mu A.cm^{-2}$ as against a value of 0.69 $\mu A.cm^{-2}$ in the chloride solution without chromates. Further, the alloy AA6056 has been found to show very low currents in the anodic region, when compared to the relatively active dissolutions observed in the other two regions. In terms of inhibition efficiency, the effect of chromate film has been observed to marginally inferior when compared to situations wherein chromates in solution as inhibitors for AA6056 alloy. However, the inhibition efficiency values for the chromated AA7075 and weld nugget regions were very relatively lower when compared that when chromates were used as inhibitors in solution.

In order to understand the pitting behaviour and also to determine the electrochemical parameters, the different regions of this dissimilar weldment were subjected to potentiodynamic polarisation studies in 3.5% NaCl solution containing 0.01M NaOH. With higher alkalinity prevailing in the solution, the

specimens, upon immersion, instantly undergo corrosion and form a thin film on the surface. The samples exhibited active-passive behaviour in this test solution. Alloy AA7075 showed a higher critical current density when compared to the other two regions, and the critical potential was nearly the same for all the three regions. In terms of passivation current density, there was not much of difference observed (**Figure 12**) in these regions, and the stable passive current density value in the range 0.30 $mA.cm^{-2}$–0.35 $mA.cm^{-2}$ was registered. The three regions have shown distinctly different breakdown potentials and protection passivation potentials. As can be seen from the electrochemical data presented in **Table 6**, the alloy AA6056 has superior pitting resistance in 3.5% NaCl test solution. Both the weld nugget/TMAZ region and the AA7075 alloy have registered a near-similar pitting potential. However, the protection potential of the weld nugget/TMAZ region was found to be marginally inferior when compared to the rest of the regions.

The results of the tests performed indicated that the beneficial effects of chromates and molybdate in imparting a better corrosion resistance for the AA6056 alloy parent material. The addition of cerium nitrate seems to have no influence on the general corrosion resistance of this alloy, despite the fact that there was a shift in the corrosion potential towards the nobler side. The pitting potential in alkaline chloride solution matches with the anodic regions of the other conditions, wherefrom activation controlled dissolution was found to begin. In the case of the AA7075 parent material, the influence of chromate was much more significant than molybdate and cerate. In terms of pitting behaviour, the potential has been observed to lie close to the rest potential of the alloy in the 3.5% NaCl solution, excepting for the case in cerium nitrate containing solution. In the case of the weld nugget/TMAZ region, all the three

inhibitors have been observed to provide a reasonably good inhibition, with efficiencies in the range between 87% and 97%.

The electrochemical studies on the different regions of the dissimilar friction stir weldment, performed in 3.5% solutions suggest that chromates are better in terms of inhibition efficiency, and a more or less similar beneficial effect on the corrosion resistance is received by all the regions by the addition of this inhibitor. From the view point of environmental issues both molybdate and cerate can be thought of as inhibitors, however, their efficiency levels are far below that of chromates in neutral chloride environments.

Conclusions

- The weld nugget has variations in chemistry, suggesting that this region a mechanical mixture of recrystallised grains of AA6056 and AA7075 alloys.
- The weld nugget/TMAZ regions with more active rest potentials may become susceptible to galvanic corrosion and undergo dissolution when the weldment is exposed to chloride environments.
- The general corrosion resistance of the AA6056 parent material is better than the AA7075 parent material and nugget/TMAZ region in chloride environments.
- The introduction of chromates into the chloride test solution as inhibitor has a better effect in terms of corrosion protection than molybdate and cerium nitrate.
- In terms of pitting tendency, both the AA7075 alloy and the nugget/TMAZ regions are equally susceptible, and that of the AA6056 alloy is marginally better.

References

1. Thomas.W.M., E.D.Nicholas, J.C.Needham, M.Murch, P.Temple-Smith, C.J.Dawes : (1991) EU Patent 0615 480 B1.
2. Thomas.W.M., E.D.Nicholas : Friction stir welding for the transportation industries, Materials and Design, 18 (1997) 269.
3. Vaidya.W.V., K.Angamuthu, V.Ventzke, M.Kocak, F.Palm : Fatigue and fracture behaviour of friction stir welded aluminium alloy AA6056-T6, Fatigue of Aeronautical Structures as an Engineering Challenge, The 22nd Symposium, International Committee on Aeronautical Fatigue (ICAF-2003), Lucerne, Switzerland, 5-9 May 2002.

4. Liu.H., H.Fujii, M.Maeda, K.Nogi : Tensile properties and fracture locations of friction stir welded joints of 6061-T6 aluminium alloy, Journal of Materials Science Letters, 22 (2003) 41.
5. Lee.W.B., Y.M.Yeon, S.B.Jung : The improvement of mechanical properties of friction stir welded A356 Al alloy, Materials Science and Engineering, A355 (2003) 154.
6. Liu.G., L.E.Murr, C.S.Niou, J.C.McClure, F.R.Vega : Microstructural aspects of the friction stir welding of 6061-T6 aluminium, Scripta Materialia, 37 (1997) 355.
7. Rhodes.C.G., M.W.Mahoney, W.H.Bingel, R.A.Spurling, C.C.Bampton : Effects of friction stir welding on microstructure of 7075 aluminium, Scripta Materialia, 36 (1997) 69.
8. Hwang.R.Y., C.P.Chou : The study on microstructural and mechanical properties of weld heat affected zone of 7075-T651 aluminium alloy, Scripta Materialia, 38 (1998) 215.
9. Salem.H.G. : Friction stir weld evolution of dynamically recrystallised AA2095 weldments, Scripta Materialia, 49 (2002) 1103.
10. Li.Y., L.E.Murr, J.C.McClure : Solid state flow visualisation in the friction stir welding of 2024 Al to 6061 Al, Scripta Materialia, 40 (1999) 1041.
11. Shigematsu.I., Y.J.Kwon, K.Suzuki, T.Imai, N.Saito : Joining of 5083 and 6061 aluminium alloys by friction stir welding, Journal of Materials Science Letters, 22 (2003) 353.
12. Corral.J., E.A.Trillo, Y.Li, L.E.Murr : Corrosion of friction stir welded aluminium alloys 2024 and 2195, Journal of Materials Science Letters, 19 (2000) 2117.
13. Pao.P.S., S.J.Gill, C.R.Feng, K.K.Sankaran : Corrosion fatigue crack growth in friction stir welded Al7050, Scripta Materialia, 45 (2001) 605.
14. Zucchi.F., G.Trabanelli, V.Grassi : Pitting and stress corrosion cracking resistance of friction stir welded AA5083, Materials and Corrosion, 52 (2001) 853.
15. Marikkannu. C., P.Bala Srinivasan, S.Sathiyanarayanan, K.Balakrishnan: Evaluation of chromate films by electrochemical impedance spectroscopy, Transactions of Institute of Metal Finishing, 73 (1995) 34.
16. Guillaumin.V., G.Mankowski : Localised corrosion of 6056 T6 aluminium alloy in chloride media, Corrosion Science, 42 (2000) 105.
17. Yue.T.M., L.J.Yan, C.P.Chan, C.F.Dong, H.C.Man, G.K.H.Pang : Excimer laser surface treatment of aluminium alloy AA7075 to improve corrosion resistance, Surface and Coatings Technology, 179 (2004) 158
18. Badawy.W.A., F.M.Al-Kharafi, A.S.El-Azab : Electrochemical behaviour and corrosion inhibition of Al, Al-6061 and Al-Cu in neutral aqueous solutions, Corrosion Science, 41 (1999) 709.
19. Brett.C.M.A., I.A.R.Gomes, J.P.S.Martins : Inhibition of aluminium corrosion in chloride media: An impedance study, Journal of Applied Electro-chemistry, 24 (1994) 1158
20. Abd Rabbo.M.J., J.A.Richardson, G.C.Wood : Study of barrier film growth on aluminium in solutions of film-promoting and aggressive ions using secondary ion mass spectrometry, Corrosion Science, 15 (1975) 689.

21. McCafferty.E., M.K.Bernett, J.S.Murday : XPS study of passive film formation on iron in chromate solutions, Corrosion Science, 28 (1988) 559.
22. Pourbaix.M : Atlas of Electrochemical Data in Aqueous Solutions, NACE, CEBELCOR, 1974, p278.
23. Liu.Y., P.Skeldon, G.E.Thompson, H.Habazaki, K.Shimizu : Chromate conversion coatings on aluminium-copper alloys, Corrosion Science, 47 (2005) 341.

Acknowledgements

The authors thank Ms Petra Fischer for the support in metallography and Dr Song for EDS analysis. One of the authors (PBS) thanks the Department of Science and Technology, New Delhi, India for awarding BOYSCAST fellowship.

Table 1
Electrochemical data for the different regions of friction stir weldment in 3.5% NaCl solution

Region	E_{corr}, mV vs. SCE	i_{corr}, μA.cm^{-2}
AA6056 base material	-658.3	0.69
AA7075 base material	-747.2	3.71
Weld nugget/TMAZ	-783.0	3.32

Table 2
Electrochemical data for the different regions of friction stir weldment in 3.5% NaCl solution containing 0.2% Na_2CrO_4 and 0.3% $Na_2Cr_2O_7$

Region	E_{corr}, mV vs. SCE	i_{corr}, μA.cm^{-2}	Inhibition η, %
AA6056BM	-738.3	0.045	93.48
AA7075 BM	-788.6	0.063	98.30
Weld nugget/TMAZ	-808.1	0.084	97.47

Table 3
Electrochemical data for the different regions of friction stir weldment in 3.5% NaCl solution containing 0.5% sodium molybdate

Region	E_{corr}, mV vs. SCE	i_{corr}, μA.cm^{-2}	Inhibition η, %
AA6056	-735.9	0.16	76.81
AA7075	-741.9	1.08	70.89
Weld nugget/TMAZ	-824.3	0.22	93.37

Table 4
Electrochemical data for the different regions of friction stir weldment in 3.5% NaCl solution containing 0.01M cerium nitrate

Region	E_{corr}, mV vs. SCE	i_{corr}, $\mu A.cm^{-2}$	Inhibition η, %
AA6056	-590.4	0.45	34.78
AA7075	-648.2	0.38	89.73
Weld nugget/TMAZ	-632.6	0.41	87.65

Table 5
Electrochemical data for the different regions of friction stir weldment in chromated condition in 3.5% NaCl solution

Region	E_{corr}, mV vs SCE	i_{corr}, $\mu A.cm^{-2}$	Inhibition η, %
AA6056	-717.3	0.048	93.04
AA7075	-745.9	0.314	91.53
Weld nugget/TMAZ	-773.5	0.437	86.84

Table 6
Electrochemical data for the different regions of friction stir weldment in 3.5% NaCl solution containing 0.01M NaOH

Region	E_{corr}, mV vs. SCE	i_{corr}, $\mu A.cm^{-2}$	i_{crit}, $\mu A.cm^{-2}$	E_{pit}, mV vs. SCE	E_{prot}, mV vs. SCE
AA6056	-1379.1	102.7	412.8	-655.2	-709.4
AA7075	-1396.0	112.8	827.1	-752.4	-794.0
WN/TMAZ	-1374.5	109.2	487.6	-771.2	-843.6

FIGURE CAPTIONS

Figure 1 Optical micrographs of base materials
(a) 6056 (b) 7075

Figure 2 Macro photograph of the dissimilar weld joint showing the features of weld nugget and adjoining regions
(AS –Advancing side, RS – Retreating side)

Figure 3 Microstructural features of friction stir weldment
(a) Weld nugget – TMAZ interface in AA6056 side
(b) Weld nugget – TMAZ interface in AA7075 side

Figure 4 Optical micrograph showing the features of the weld nugget

Figure 5 Higher magnification micrographs of regions marked (a) & (b) in Figure 4
(a) Region 'a' (b) Region 'b'

Figure 6 EDS line scan across the friction stir weld nugget

Figure 7 Potentiodynamic polarisation behaviour of FS weldment in 3.5% NaCl solution

Figure 8 Potentiodynamic polarisation behaviour of FS weldment in 3.5% NaCl solution containing 0.2% Na_2CrO_4 and 0.3% $Na_2Cr_2O_7$

Figure 9 Potentiodynamic polarisation behaviour of FS weldment in 3.5% NaCl solution containing 0.5% sodium molybdate

Figure 10 Potentiodynamic polarisation behaviour of FS weldment in 3.5% NaCl solution containing cerium nitrate

Figure 11 Potentiodynamic polarisation behaviour of chromated FS weldment in 3.5% NaCl solution

Figure 12 Potentiodynamic polarisation behaviour of FS weldment in 3.5% NaCl solution with 0.01 M NaOH

TABLE CAPTIONS

Table 1 Electrochemical data for the different regions of friction stir weldment in 3.5% NaCl solution

Table 2 Electrochemical data for the different regions of friction stir weldment in 3.5% NaCl solution containing 0.2% Na_2CrO_4 and 0.3% $Na_2Cr_2O_7$

Table 3 Electrochemical data for the different regions of friction stir weldment in 3.5% NaCl solution containing 0.5% sodium molybdate

Table 4 Electrochemical data for the different regions of friction stir weldment in 3.5% NaCl solution containing 0.01M cerium nitrate

Table 5 Electrochemical data for the different regions of friction stir weldment in chromated condition in 3.5% NaCl solution

Table 6 Electrochemical data for the different regions of friction stir weldment in 3.5% NaCl solution containing 0.01M NaOH

Non-colour figure
Click here to download high resolution image

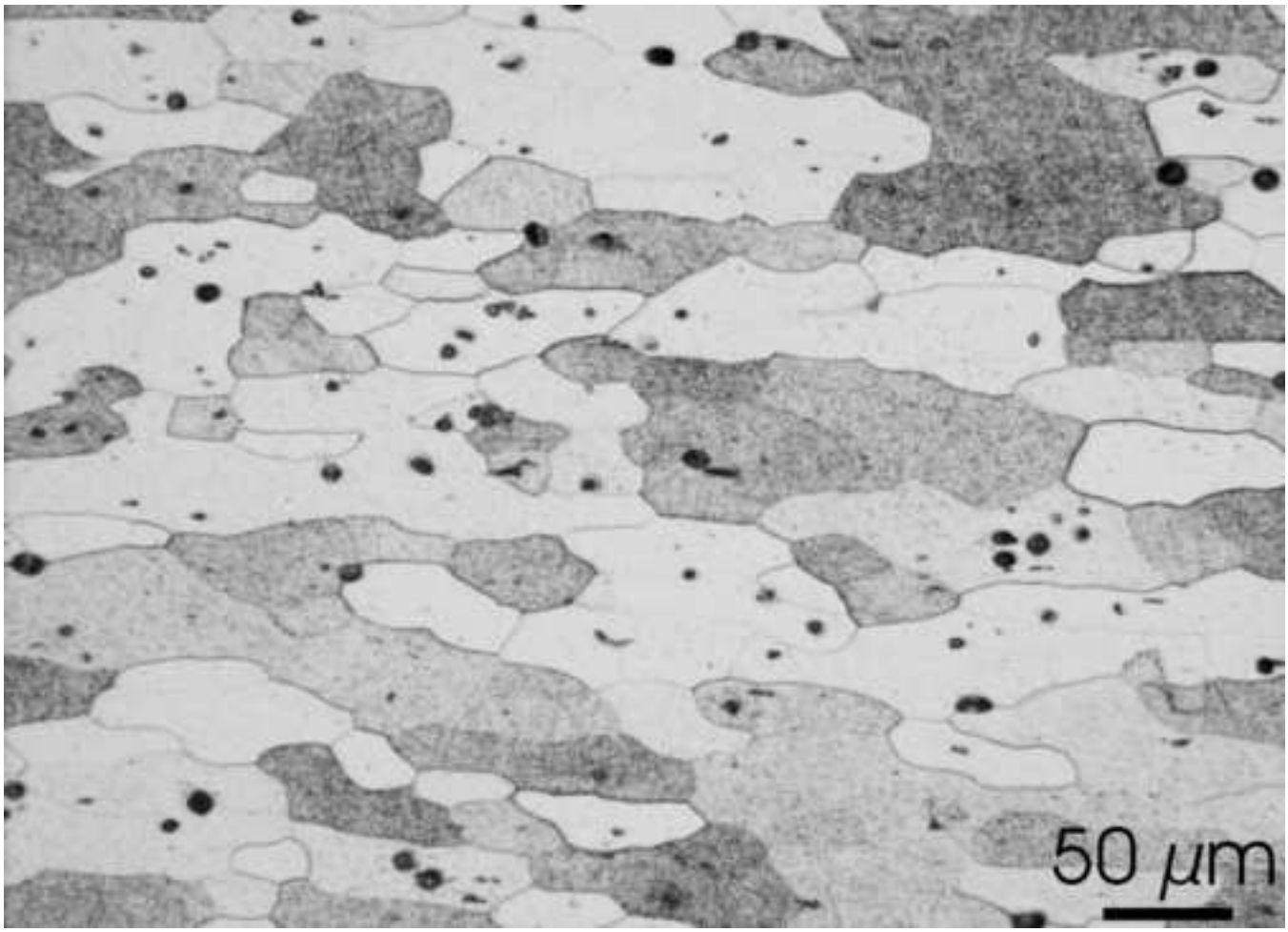

Non-colour figure
Click here to download high resolution image

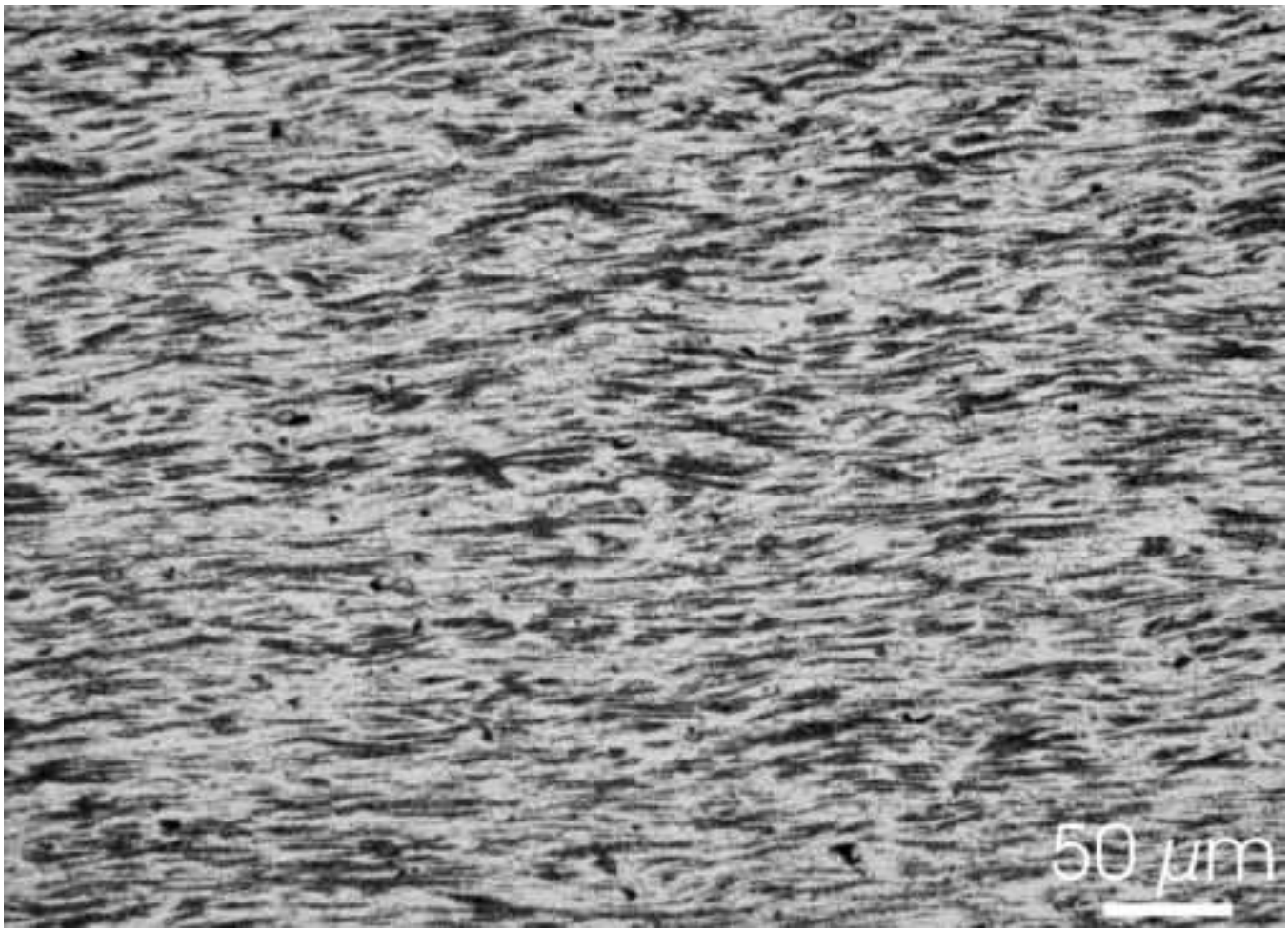

Non-colour figure
Click here to download high resolution image

Non-colour figure
Click here to download high resolution image

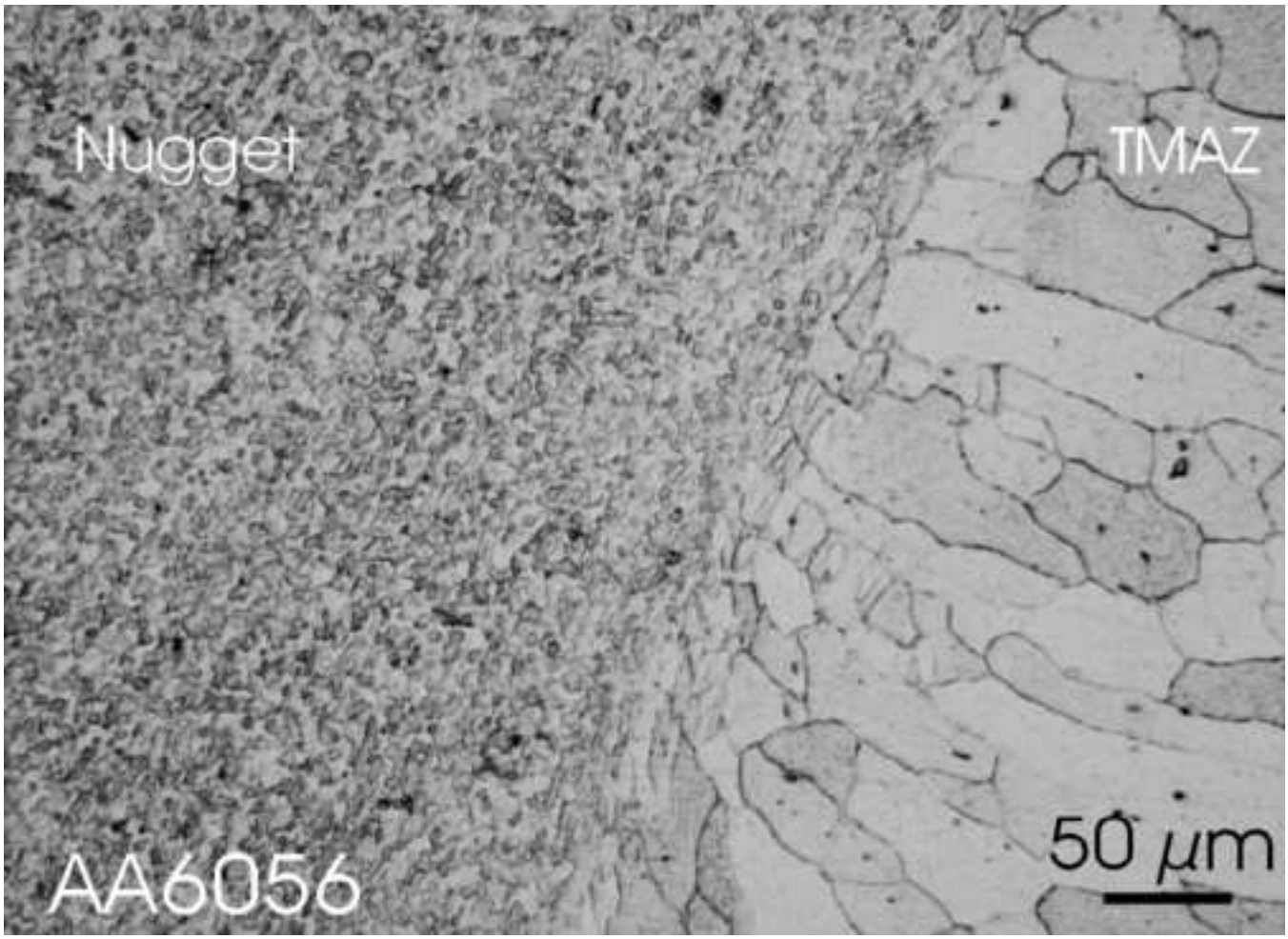

Non-colour figure
Click here to download high resolution image

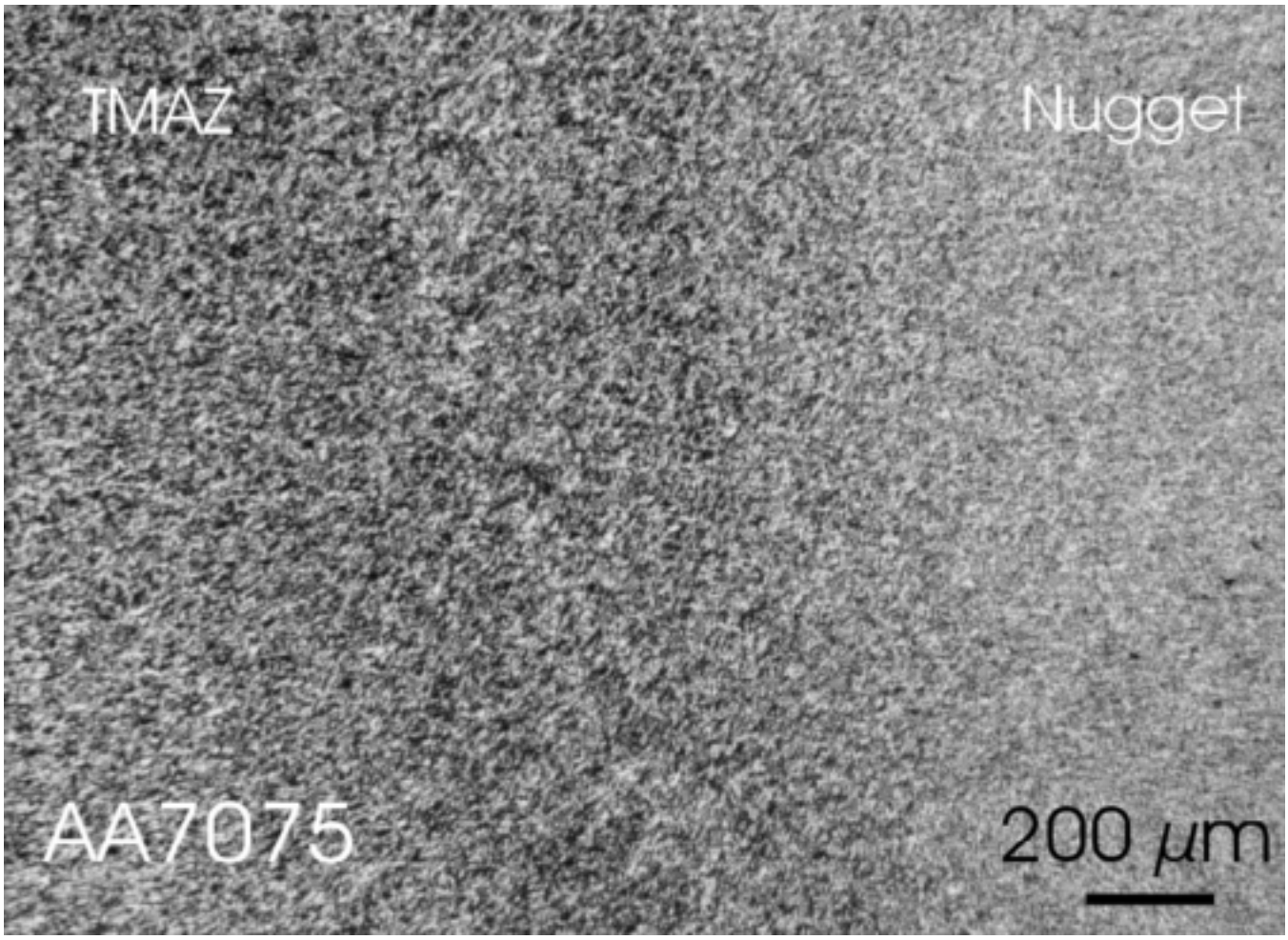

Non-colour figure
Click here to download high resolution image

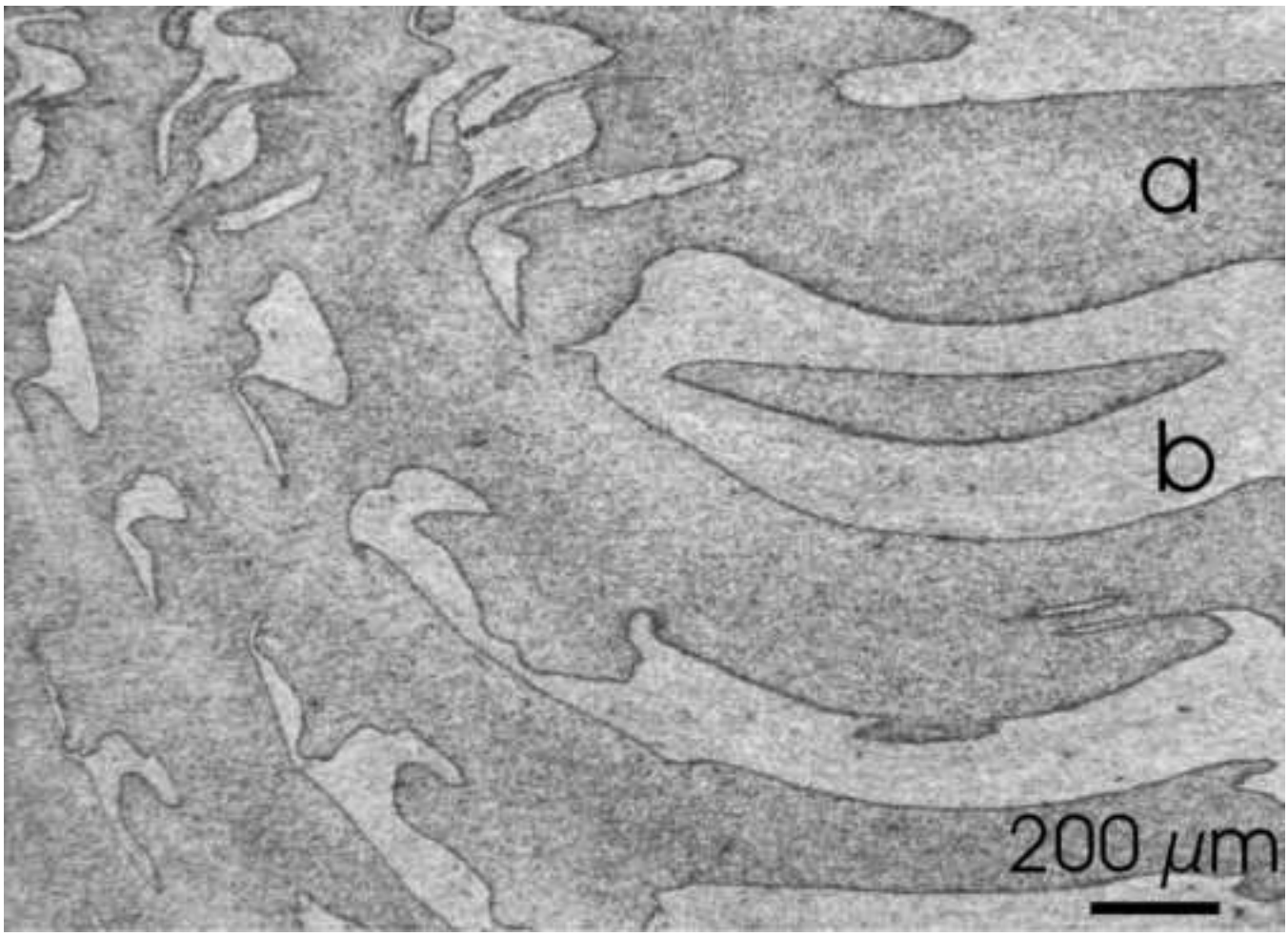

Non-colour figure
Click here to download high resolution image

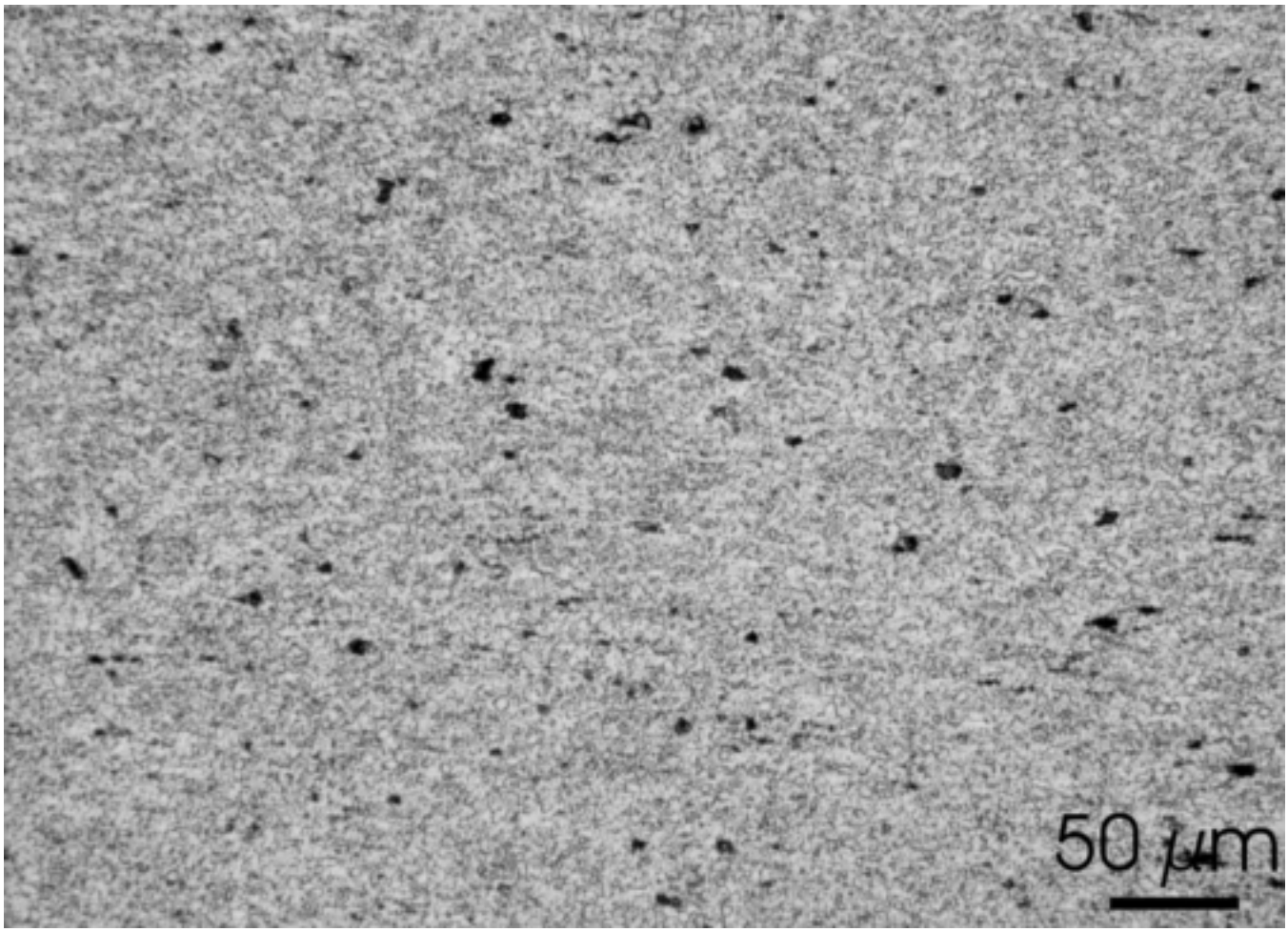

Non-colour figure
Click here to download high resolution image

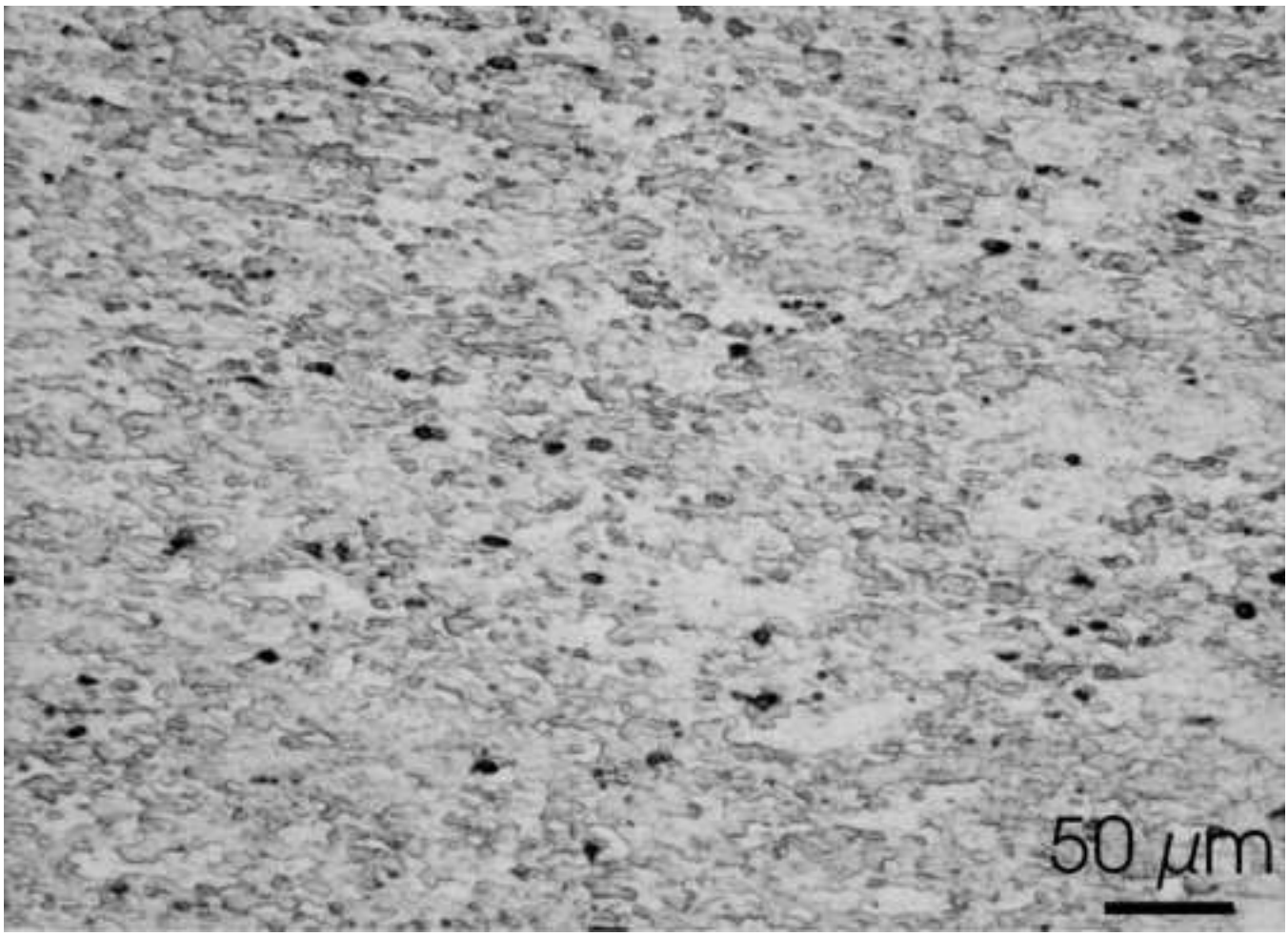

Non-colour figure

Click here to download high resolution image

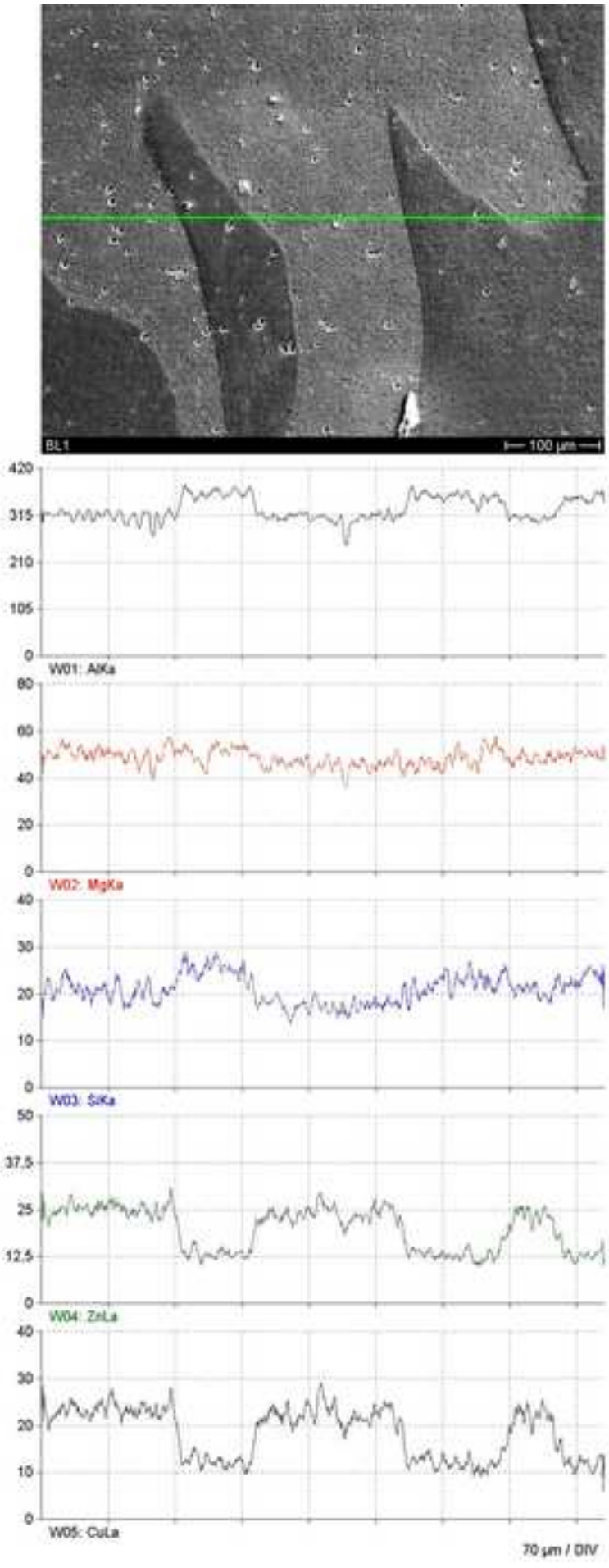

Non-colour figure
Click here to download high resolution image

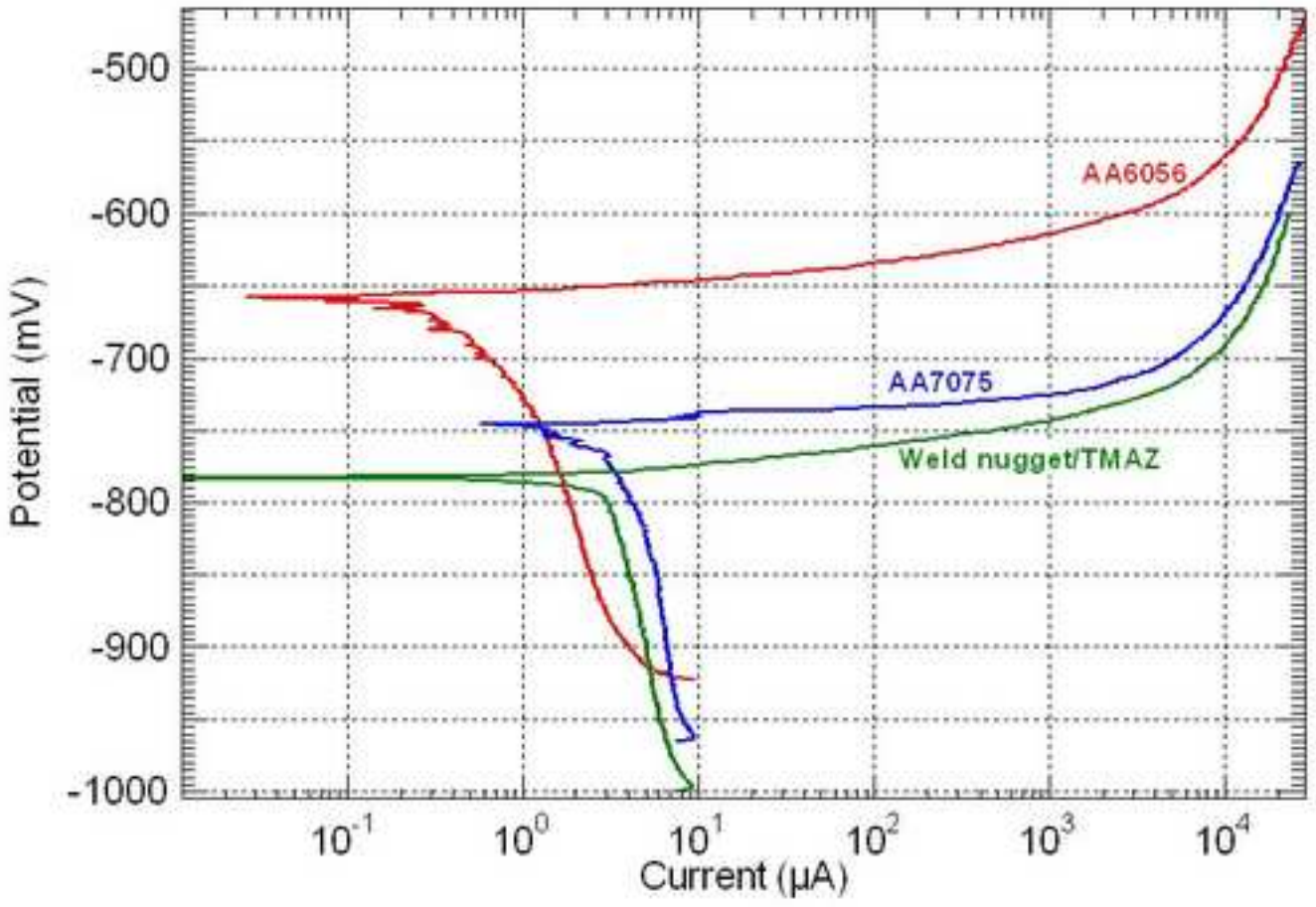

Non-colour figure
Click here to download high resolution image

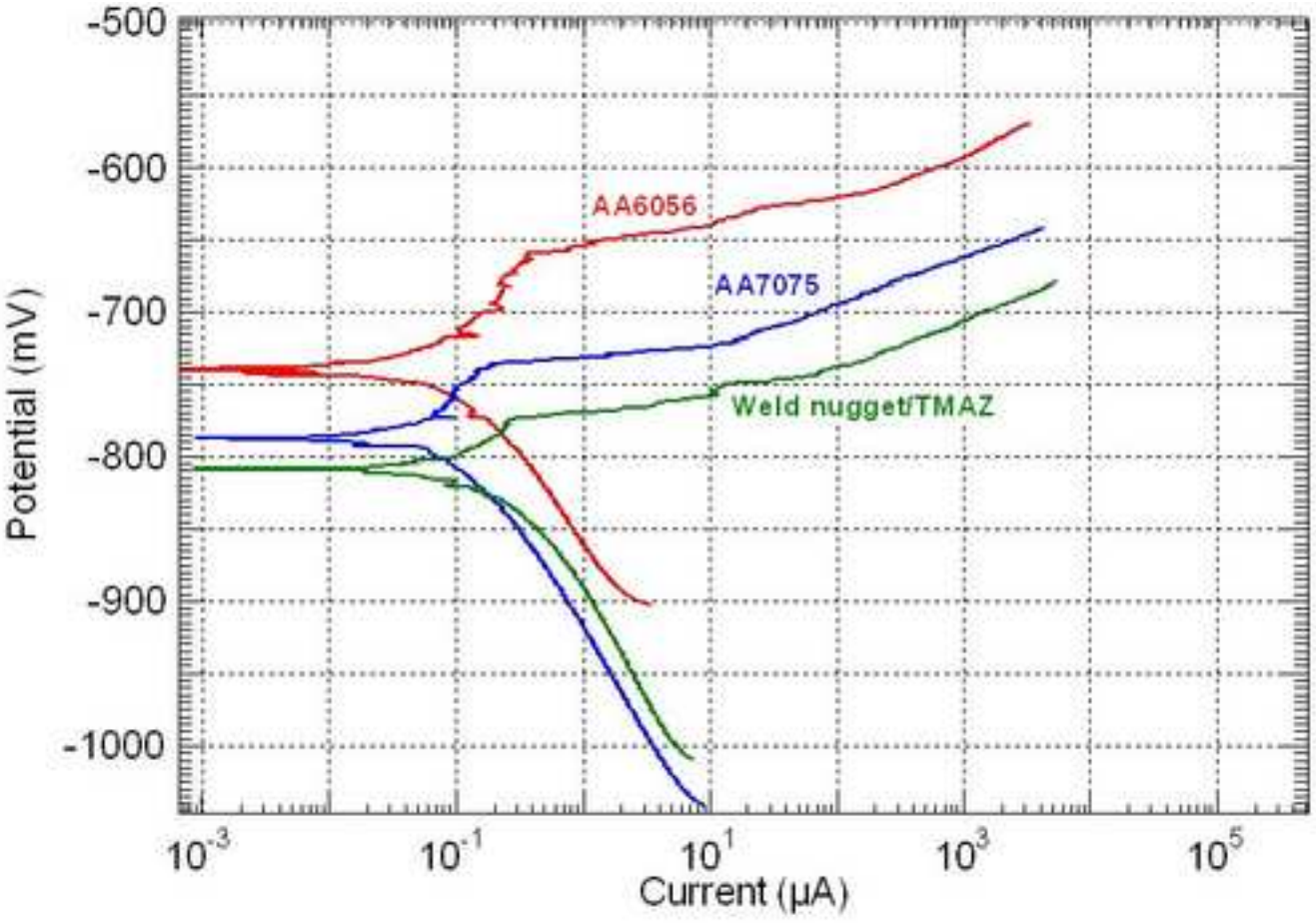

Non-colour figure
Click here to download high resolution image

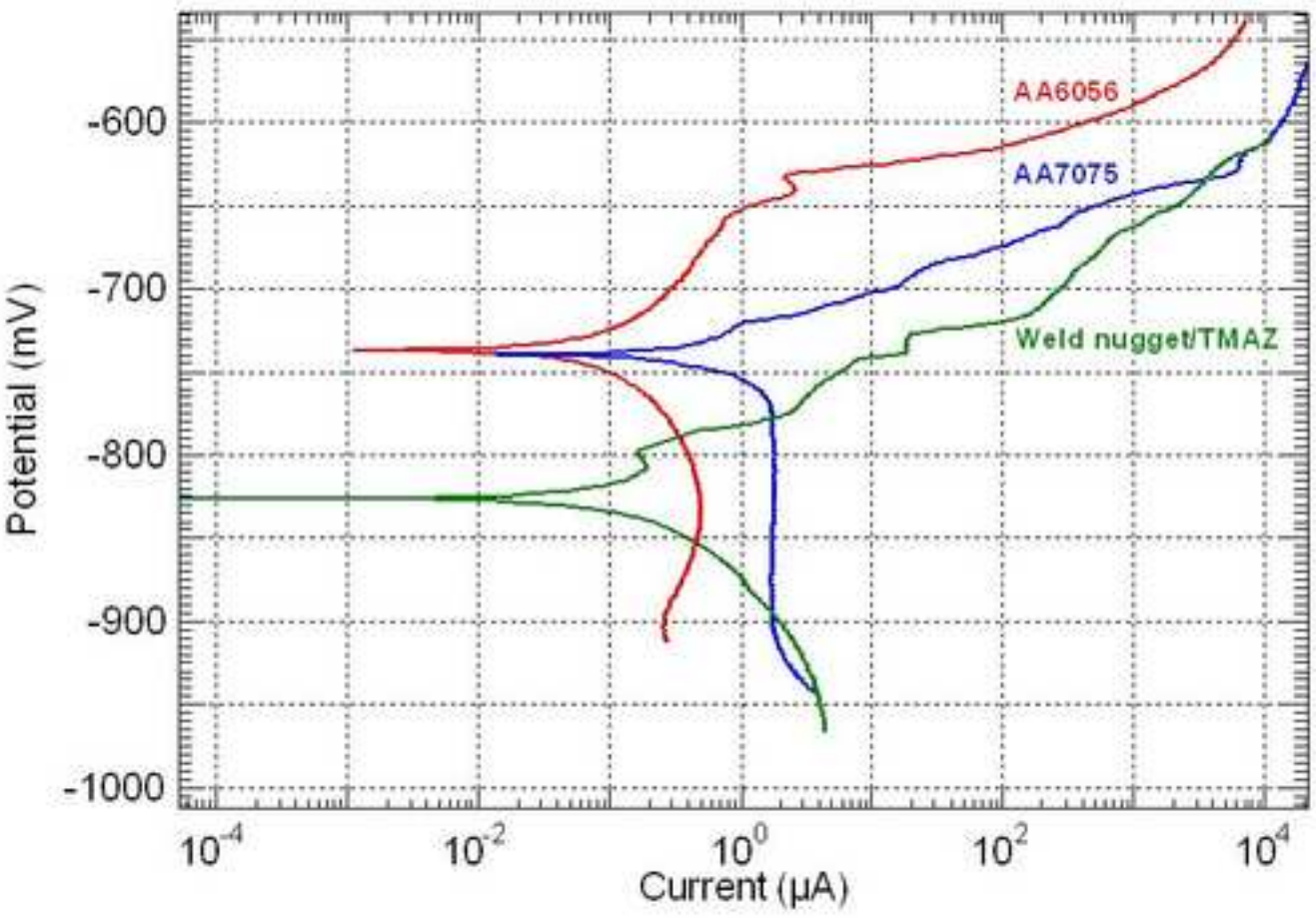

Non-colour figure
Click here to download high resolution image

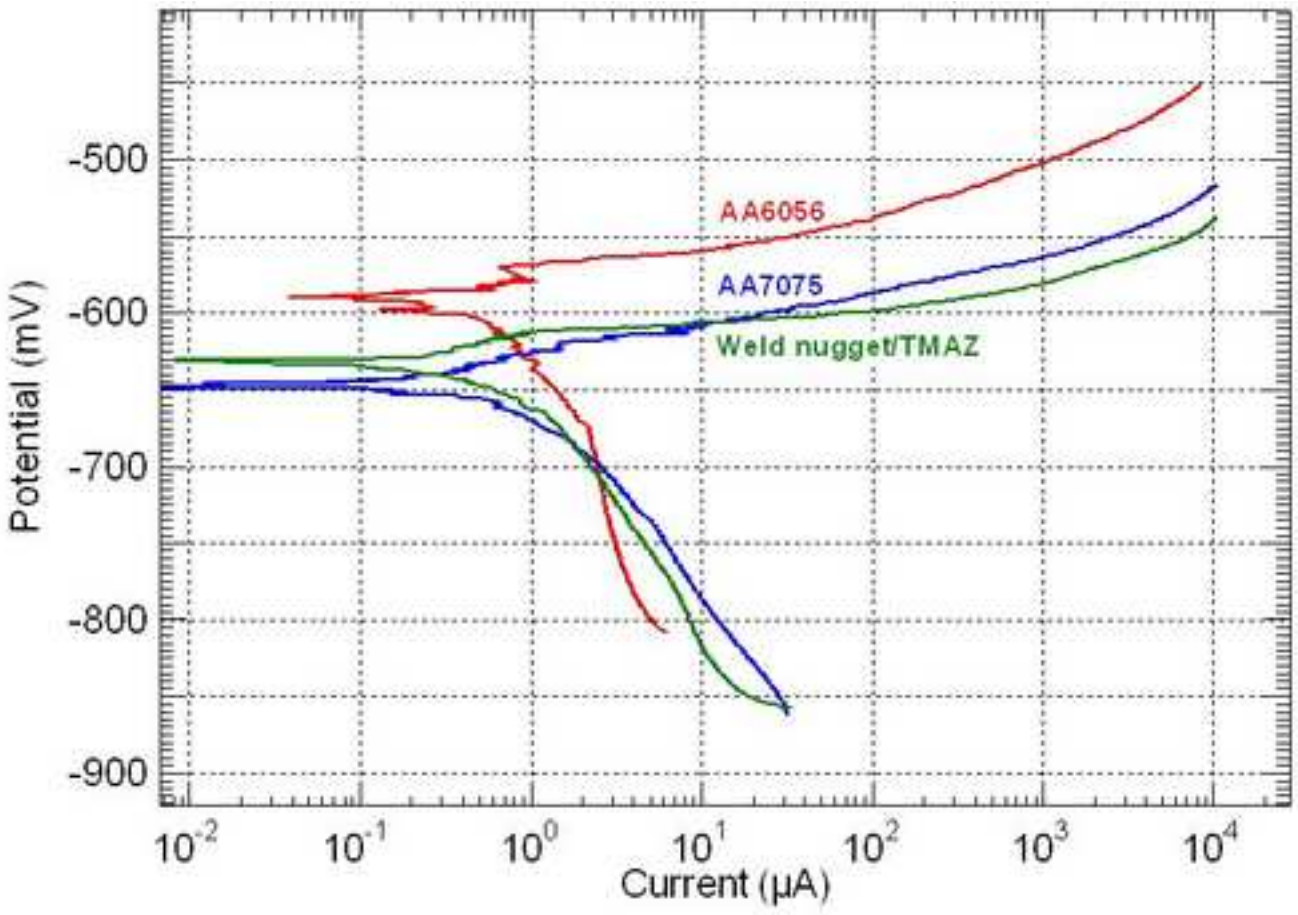

Non-colour figure
Click here to download high resolution image

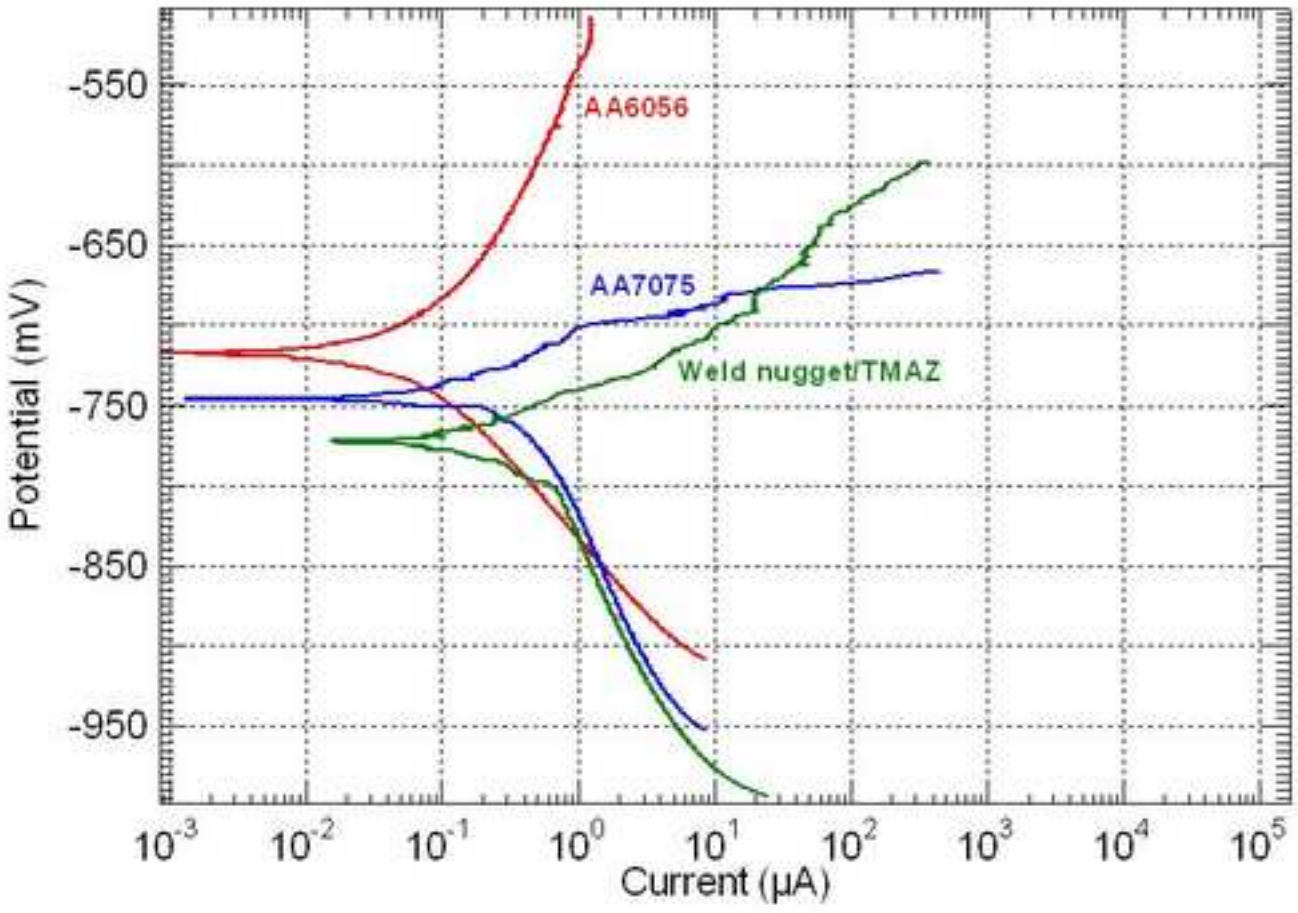

Manuscript

Click here to download high resolution image